Study on hydrophobic modification of basil seed gum-based (BSG) films by octenyl succinate anhydride (OSA)

Hadi Hashemi Gahruie[a], Mohammad Hadi Eskandari[a], Paul Van der Meeren[b], Seyed Mohammad Hashem Hosseini[a],*

[a] Department of Food Science and Technology, School of Agriculture, Shiraz University, Shiraz, Iran
[b] Particle and Interfacial Technology Group, Faculty of Bioscience Engineering, Ghent University, Coupure Links 653, B-9000 Gent, Belgium

ABSTRACT

The main objective of this study was to evaluate the changes in the characteristics of basil (*Ocimum bacilicum* L.) seed gum (BSG) films after modification with octenyl succinate anhydride (OSA) at different OSA:BSG weight ratios (WRs) of 0, 0.01 and 0.03. HPLC analysis revealed that the amount of added OS groups was 0%, 0.28%, and 1.01%, respectively. The introduction of OS groups along the BSG backbone was also confirmed by FT-IR and NMR analysis. XRD results revealed no significant change of physical state after modification. The contact angle (i.e., hydrophobicity) of modified BSG films was higher than that of control film. A decrease in the film solubility in water (29%) and water vapor permeability (50%), but an increase in density (14.28%) and opacity (21.37%) was observed after modification at the WR of 0.03. Also, the results showed that modification with OSA had no significant influence on the film thickness, moisture content and color properties. BSG modification with OSA at the WR of 0.03 significantly increased the flexibility and ultimate strength of respective films. The results of this study showed that OSA-modified BSG is a good candidate for developing edible films and coating with relatively high resistance to water.

1. Introduction

The quick increase in the production rate of non-degradable petroleum-based plastic materials causes serious environmental concerns (Debeaufort, Quezada-Gallo, & Voilley, 1998). Therefore, many efforts have been made to find environmentally friendly materials. Natural polymers (proteins and polysaccharides) have received much attention due to their biodegradability (Janjarasskul & Krochta, 2010). However, the application of biopolymers in developing packaging materials is almost limited due to their inherent hydrophilic nature, poor moisture barrier properties and inappropriate mechanical properties (Zúñiga, Skurtys, Osorio, Aguilera, & Pedreschi, 2012).

Different strategies (like incorporating hydrophobic ingredients, cross-linking, and formation of nanocomposite films) have been utilized to improve the water vapor barrier and mechanical properties of biopolymer-based films (Konwar, Gogoi, Majumdar, & Chowdhury, 2015; Thakur et al., 2016; Yang et al., 2017). Incorporating hydrophobic ingredients such as waxes and fatty acids results in excellent water vapor barrier properties but increases the opacity and brittleness of film network (Chao, Yue, Xiaoyan, & Dan, 2010; Sagiri et al., 2014). Because

of low miscibility, formation of physically stable film forming emulsions prior to drying is also challenging. Network cross-linking using either different types of cross-linkers or irradiation is another method to improve the characteristics of bio-based films (Benbettaïeb, Karbowiak, Brachais, & Debeaufort, 2016; Yang et al., 2017). However, some cross-linkers suffer from high toxicity (Xu, Canisag, Mu, & Yang, 2015).

Chemical modification of biopolymer chains is a promising method to reduce the hydrophilic character of hydrocolloids without significant changes in bulk composition. The hydroxyl groups along the biopolymer backbone are esterified with hydrophobic molecules to decrease the water sensitivity of the resultant film network (Ali, Bijalwan, Basu, Kesarwani, & Mazumder, 2017; Ren et al., 2016; Ren et al., 2010).

There has been an increasing interest in the simple chemical modification of different hydrocolloids, especially starch, to improve their hydrophobic properties using octenyl succinate anhydride (OSA) and dodecenyl succinate anhydride (DSA). Abiddin, Yusoff, and Ahmad (2018) studied the physicochemical, thermal, and morphological properties of sago starch modified with OSA. Zhou, Ren, Tong, and Ma (2009) and Zhou, Ren, Tong, Xie, and Liu (2009) studied the modification of corn starch using OSA and DSA, respectively. Biswas,

---

Selling, Woods, and Evans (2009) studied the modification of zein using OSA and alkyl (or alkenyl) ketene dimers. Generally, improvements in the interfacial and hydrophobic properties have been reported after modification with OSA and DSA.

As a thickener, basil seed gum (BSG) has some advantages such as biocompatibility, low production cost, and edibility which make BSG a useful hydrocolloid for developing edible coatings and films (Gahruie, Ziaee, Eskandari, & Hosseini, 2017; Hashemi Gahruie, 2019). Similar to most biopolymer-based edible films, BSG films suffer from the high solubility in water, which limit their application when the product integrity is important (e.g., in humid conditions) (Hosseini, Razavi, & Mousavi, 2009). The high water sensitivity also affects the mechanical properties. The hydrophilic characteristic is due to the presence of hydroxyl groups along the BSG backbone (Khazaei, Esmaiili, Djomeh, Ghasemlou, & Jouki, 2014).

To our knowledge, the focus of the most published reports regarding the modification with OSA is on improving the interfacial (emulsifying and foaming) properties of starch granules obtained from different sources. The OSA modification of hydrocolloids other than starch is almost limited. Moreover, the chemical modification of BSG with OSA has not been reported yet. The main objective of this work was evaluating the effect of BSG modification with OSA on different properties of BSG-based films.

2. Materials and methods

2.1. Materials

Basil seed gum (BSG) was obtained from Reyhan Gum Parsian (Tehran, Iran). 2-Octen-1-ylsuccinic anhydride (OSA, 97% purity) was purchased from Sigma-Aldrich (St. Louis, MO, USA). HPLC-grade acetonitrile and methanol were purchased from Merck Co. (Darmstadt, Germany). Pure canola oil was kindly donated by Narges Shiraz Company (Shiraz, Iran). All other chemicals were of analytical grade and used without further purification.

2.2. Modification of basil seed gum

BSG was modified with OSA using the method described by Pan, Yang, and Qiu (2015) with some modifications. A BSG dispersion (1.5% w/v) was prepared in deionized water and hydrated overnight. After that, the pH was adjusted to pH 8.0 using 0.5 M NaOH solution. Ethanolic solution of OSA was added to BSG dispersion at 25 °C to reach different OSA:BSG weight ratios (WR) of 0, 0.01 and 0.03. OSA and BSG were then allowed to react at 40 ± 2 °C for 90 min while maintaining the pH at 8.0. The reaction was terminated by the addition of 0.1 M HCl to pH 6.0. Washing with absolute ethanol was performed three times to remove the residual amounts of free OSA. The precipitates were then freeze-dried. The modified samples were named as S0, S1 and S3 indicating the WRs of 0, 0.01 and 0.03 during modification, respectively.

2.3. Determination of the extent of modification

The amount of bound OS was determined according to the method described by Shi et al. (2017) with slight modifications. Exactly 100.0 mg of dry sample was immersed in 2 mL of NaOH (4 M) and stirred overnight. The alkali treated solutions (0.4 mL) were mixed with 3.6 mL of 1 M HCl and then made to volume with acetonitrile in a 5 mL volumetric flask. The samples were then analyzed using an HPLC system (Knauer, Germany) equipped with Smartline pump 1000 and C18 column (sphere image 80-5 ODS 2, particle size 5 μm, length 300 mm, inner diameter 4 mm, Knauer, Germany). A mixture of acetonitrile and water (50:50 v/v) containing 0.1% formic acid was used as the mobile phase (flow rate 0.8 mL/min). Samples were filtered through 0.45 μm syringe filters and then injected (10 μL). The UV absorption was measured at 200 nm using 2100 UV detector (Knauer, Germany).

The OS content was calculated from the OSA standard curve ($y = 2739.4x + 113801$) constructed by plotting the peak area vs. different OSA concentrations (μg/mL). The amount of bound OS (%) was calculated using Eq. (1).

$$\%OS = (250W_t/W) \times 100 \tag{1}$$

where, W is the dry weight (g) of sample, W_t is the OS content determined from the standard curve, and 250 is the dilution factor.

2.4. Fourier-transform infrared spectroscopy

Different BSG samples were mixed with KBr to prepare pellets. The spectrum was obtained by Thermo Nicolet Avatar 370 spectrometer (Thermo Nicolet Corp., Madison, WI, USA) in the wavenumber range of $4000–400\ cm^{-1}$.

2.5. ^1H NMR spectroscopy

^{1}H NMR spectroscopy of BSG samples was performed according to the method described by Nie et al. (2013). Hydrocolloid dispersions (˜0.1%, w/v) were prepared in a mixture of deuterated D_2O:DMSO (1:1) and kept at room temperature for 24 h. ^{1}H NMR spectra were recorded at 25 °C using a Bruker Avance DPX 250 MHz (Karlsruhe, Germany).

2.6. X-ray diffraction

X-ray diffraction (XRD) analysis of gum samples was performed using an X-ray powder diffractometer (Bruker AFX D8, Germany) with Cu Kα radiation (λ = 0.154056 nm) at 25 °C, 40 kV, and 40 mA. Diffractograms were obtained from 2θ from 5-70° in 0.05° step and 1 s step time.

2.7. Preparation of films

BSG dispersions (1% w/w) were prepared in double distilled water (DDW) containing glycerol (0.6% w/w) as the plasticizer. Before hydration, the dispersion was mixed by a dispenser/homogenizer (HG-15D, Daihan Scientific, Seoul, Korea) at 3200 rpm for 1 min. Hydration was completed on a roller mixer for 24 h. To remove the gas bubbles, the film forming solutions (FFSs) were subjected to vacuum deaeration for 30 min. FFSs (25 g) were casted onto Teflon plates (48 cm²) and dried at room temperature during 24–48 h. Dried films were peeled off and conditioned at 25 °C and 53% relative humidity (RH) in hermetic boxes containing saturated $Mg(NO_3)_2$ solution.

2.7.1. Film thickness and density

A digital micrometer (Mitutoyo No. 293-766, Tokyo, Japan) was used to measure (± 0.001 mm) the film thickness in at least ten random locations. The film density was measured by dividing the weight (g) by the volume (cm³). To calculate the film volume, the surface area was multiplied by the thickness.

2.7.2. Opacity

A piece of pre-conditioned film (1 × 5 cm²) was positioned on the inner surface of a cuvette. The absorbance of the film was measured by a UV–vis spectrophotometer (UNICO UV-2100, USA) at 600 nm. Opacity was calculated using Eq. (2) (Esteghlal, Niakosari, Hosseini, Mesbahi, & Yousefi, 2016):

$$Opacity = Absorbance/I \tag{2}$$

where, I is the average film thickness (mm).

2.7.3. Moisture content

The moisture content of BSG-based films was determined using the method described by Khazaei et al. (2014). Briefly, films were dried at

110 °C to reach a constant weight. The moisture content (MC) was calculated using the following equation.

$$MC\ (\%) = \ [(M_1 - M_2)/M_1] \times 100 \tag{3}$$

where, M_1 and M_2 are wet and dry weight, respectively.

2.7.4. Solubility in water

Film solubility (%) was evaluated according to the method described by Esteghlal et al. (2016). Film cuts (1×3 cm^2) were dried overnight at 85 °C and then weighed to determine the initial solid content. Dried BSG films were stirred at 100 rpm in 50 ml DDW for 6 h at 25 °C. Subsequently, the mixtures were filtered through Whatman filter paper No. 1 to separate undissolved films. After re-drying at 85 °C (to determine the final solid content), film solubility was calculated using Eq. (4).

Film solubility (%) = [(initial solid content-final solid content)/initial solid content) × 100   (4)

2.7.5. Water vapor permeability

Water vapor permeability (WVP) was determined using the standard method of ASTM 05.11 (Testing, A. S. f., & Materials, 2013). Aluminum cups were filled with dried CaCl$_2$ (50 g) to reach 0% RH$_i$ beneath the film surface. The cups were then tightly covered with pre-conditioned BSG films and placed in a hermetic box containing saturated NaCl solution (75% RH$_o$) at 25 °C. Weighing was performed at 1-h intervals until 6 h and then at 6-h intervals until 24 h. The weight increment was plotted against time (h) and the slope was considered as water vapor transmission rate (WVTR) in g/h. WVP (g /h mm kPa) was determined using Eq. (5).

$$WVP = (WVTR \times I)/P_0 \times A \times \ (RH_o - RH_i) \tag{5}$$

where, I is the average film thickness (mm); P_0 is the saturation vapor pressure at 25 °C (1753.55 Pa); A is the film (cup) surface area (mm^2); and (RH_o–RH_i) is the difference between the relative humidity outside and inside the cups.

2.7.6. Contact angle

A water droplet formed at the tip of a needle was placed on the pre-conditioned BSG films. A CCD camera equipped with macro lens was used to take pictures of the drop shape. Analysis was performed using ImageJ software (1.44p, National Institute of Health, USA).

2.7.7. Color parameters

The color of BSG films was evaluated using the method described by Afshari-Jouybari and Farahnaky (2011) and Hosseini et al. (2019). A digital camera (Canon Powershot A540, 6 megapixels resolution) was used in a vertical position for taking photos, which were saved as jpg format. The camera was placed in a wooden box ($50 \times 50 \times 60$ cm^3) with a natural daylight source (6500 K). The interior color of the box was white. The distance between the sample and lens was 25 cm. The values of L^* (brightness), a^* (redness-greenness) and b^* (yellowness-blueness) of BSG films were determined using Adobe Photoshop® CS6. Total color difference (ΔE) with respect to standard white plate and whiteness index (WI) were determined according to the following equations.

$$\Delta E = \sqrt{(L_C^* - L_S^*)^2 + \ (a_C^* - a_S^*)^2 + (b_C^* - b_S^*)^2} \tag{6}$$

$$WI = 100 - \sqrt{(100 - L_S^*)^2 + a_S^{*2} + b_S^{*2}} \tag{7}$$

where, L_C^*, a_C^*, and b_C^* are the color parameters values of standard white plate (93.49, 0.25 and 0.09, respectively) and L_S^*, a_S^*, and b_S^* are those of BSG film samples, respectively.

2.7.8. Mechanical properties

Tensile strength and elongation at break were determined using a texture analyzer (TAXT-2i Texture Analyzer, Stable Microsystems, Surrey, England). Rectangular (10×60 mm^2) strips of pre-conditioned BSG films were subjected to tensile forces at the cross-head speed of 1 mm/s. The initial grip distance was 50 mm. Ultimate tensile strength (*TS*, kPa) and elongation at break (*EAB*%) were determined using following equations.

$$TS = \ F/A \tag{8}$$

$$EAB = \ (\Delta L/L) \times 100 \tag{9}$$

where, F (N) is the maximum force at the rupture point; A (m^2) is the cross-sectional area (thickness × width); ΔL is the increase in the length before breakage; and L is the initial length between the grips.

2.7.9. Film microstructure

The surface morphology of BSG films was evaluated using a scanning electron microscope (TESCAN vega3, Czech Republic). Film cuts, fractured in liquid nitrogen, were placed on the specimen holder using an aluminum tape and covered with a thin layer of gold (Desk Sputter Coater DSR1, Nanostructural Coating Co., Iran). Micrographs were taken at an accelerating voltage of 10 kV.

2.8. Statistical analysis

All experiments were performed in triplicate unless otherwise indicated. The results were analyzed using one-way analysis of variance at the significance level of 0.05. Duncan's multiple range tests (SAS® software, ver. 9.1, SAS Institute Inc., NC, USA) were used to determine significant differences between the means.

3. Results and discussion

3.1. The extent of esterification

Fig. 1 illustrates a schematic representation of the interaction between OSA and BSG. Modified BSG was obtained from the esterification reaction between the carboxyl group of OSA and the hydroxyl groups along BSG backbone. As determined by HPLC, the amounts of esterification were 0%, 0.28% and 1.01% at OSA:BSG weight ratios (WRs) of 0, 0.01 and 0.03, respectively. Shi et al. (2017) reported the esterification values of 0%, 0.64%, 1.09% and 1.80% at OSA to *Acacia seyal* gum WRs of 0, 0.01, 0.02, and 0.03, respectively. An increase in the emulsifying properties of Persian gum has been reported after esterification with OSA (Mohammadi, Abbasi, & Scanlon, 2016).

3.2. ^{1}H NMR spectroscopy

Fig. 2 shows the ^{1}H NMR spectrum of unmodified and modified samples. The observed peak at a chemical shift of 2.00–2.30 ppm was attributed to the acetyl groups (Meng, Zheng, Wang, Liang, & Zhong, 2014; Nie et al., 2013). This peak was also identified in the spectra of
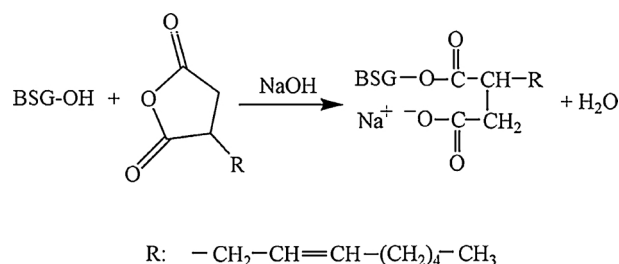

Fig. 1. Schematic representation of the esterification reaction between BSG and OSA.
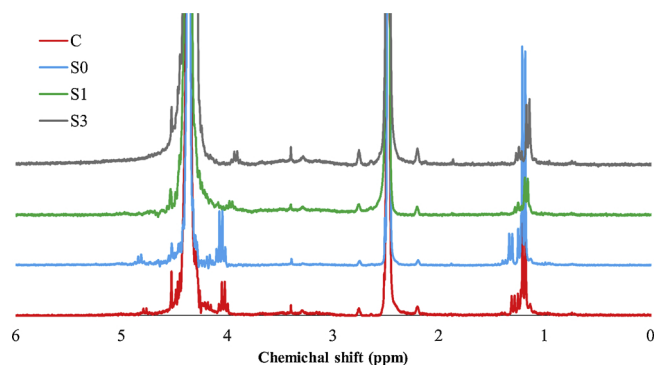
Fig. 2. ^{1}H NMR spectra of different BSG samples; C indicates unmodified sample. S0, S1 and S3 indicate the modified samples prepared at OSA:BSG weight ratios of 0, 0.01 and 0.03, respectively.

Fig. 3. FTIR spectra of different BSG samples; C indicates unmodified sample. S0, S1 and S3 indicate the modified samples prepared at OSA:BSG weight ratios of 0, 0.01 and 0.03, respectively.

Table 1

FTIR peak assignments of different BSG samples.

Assignment	Wave number (cm^{-1})			
	C	S0	S1	S3
	648.79	618.48	642.16	613.82
		776.74	779.58	
		897.90		899.23
C-O-C stretching vibrations of glycosidic bonds	1052.59	1054.12	1052.45	1053.76
C-O-C stretching vibrations of glycosidic bonds	1159.64	1161.28	1161.17	1161.04
-OH bending vibration		1244.7	1247.71	
C = N stretching vibration	1421.12	1420	1419.72	1420.34
C = C stretching vibration	1629.50	1623.33	1623.03	1620.33
	2122.33	2135.77	2138.12	2133.42
-CH$_2$- and > CH- stretching and bending vibrations	2922.12	2907.24	2907.83	2925.11
-OH stretching vibrations	3418.81	3409.22	3410.77	3423.55

C indicates unmodified sample. S0, S1 and S3 indicate the modified samples prepared at OSA:BSG weight ratios of 0, 0.01 and 0.03, respectively.

OSA-modified samples with no distinct difference in the intensity, indicating that the acetyl groups were not cleaved during modification. The NMR spectra of control BSG and that modified at OSA:BSG WR of 0 were similar to each other. In modified samples, peaks at 2.6–4 ppm were assigned to the OS group (Bai & Shi, 2011). The multiple peaks at 5.4–5.6 ppm and 0.8–1.0 ppm corresponded to the double bond proton and the terminal methyl protons of the OS group, respectively (Bai, Shi, Herrera, & Prakash, 2011). The multiple peaks at 1.14 ppm corresponded to the methylene protons on the octenyl chain of the grafted OS groups (Eenschooten, Guillaumie, Kontogeorgis, Stenby, & Schwach-Abdellaoui, 2010). Moreover, the intensities of the above-mentioned signals increased with increasing %OS. These findings indicated the grafting of OSA onto BSG molecules, which is consistent with the results obtained by FTIR.

^{1}H spectra were also helpful in determining the position of OS substitution on BSG. The ^{1}H spectra of modified BSG revealed the possible substituted positions of the OS groups in rhamnopyranosyl (Rhap). The latter hypothesis was derived from the fact that the peak of BSG and OSA (%OS, 0.28 and 1.01) at 1.15 ppm, which corresponded to the proton of CH3- Rhap (Nie et al., 2013), became broader than those of C and S0. This is consistent with the report of Bai and Shi (2011), who attributed the peak broadening at 5.38 ppm (H-1 of 1,4-linked repeated units) to the substitution of OS at the O-2 position. Simultaneously, Rhap was mainly distributed in the outer surface of BSG molecules, suggesting that OSA will more readily react with Rhap.

3.3. Fourier transform infrared (FTIR) spectroscopy

Changes in the functional groups of BSG after succinylation were studied using FTIR spectroscopy. Fig. 3 shows the FTIR spectra of unmodified BSG and those modified with OSA. The bands at around 1161 and 1052 cm^{-1} were assigned to C-O-C stretching vibrations of glycosidic bonds (Table 1). The absorption peaks at 1420 and 1628 cm^{-1} were assigned to C=N and C=C stretching vibrations, respectively. Inter- or intra-molecular hydrogen bonds are generally determined by OH stretching vibrations. Broad areas of absorption between 3500 and 3000 cm^{-1} show a number of features such as free hydroxyl groups stretching bonds and O-H bands of carboxylic acid (Kang et al., 2011). The broad absorption bands at 3000 and 2800 cm^{-1} were assigned to -CH$_2$- and > CH- stretching and bending vibrations (Kang et al., 2011). No distinct differences were observed between the unmodified BSG (denoted as C) and that modified at OSA:BSG WR of 0 (denoted as S0). Modified samples (S3) showed a new peak at 2925 cm^{-1}. This peak was more obvious in sample S3 compared to sample S1 due to the higher degree of modification. Zhou, Ren, Tong, Ma et al. (2009) studied the effect of surface esterification with OSA on the hydrophilicity of corn starch films. They reported that the intensity of the CH$_2$
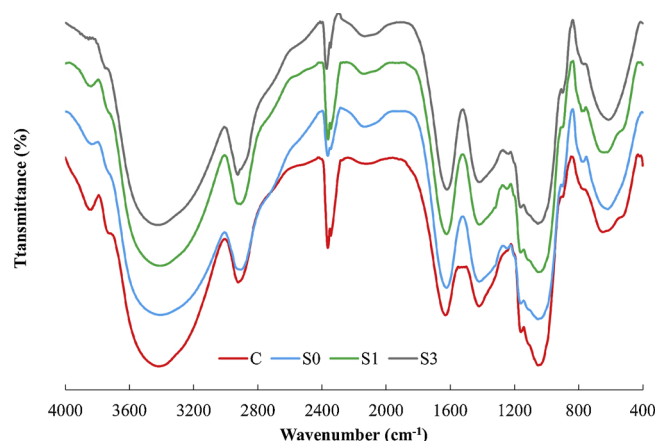
vibration (2929 cm^{-1}) in an FTIR spectrum could only give a qualitative comparison of the surface esterification.

3.4. X-ray diffraction

In order to study the effect of modification with OSA on the physical state of BSG molecules, unmodified and modified BSG samples were examined by X-ray diffraction (XRD). As shown in Fig. 4, the modified BSG samples had fairly the same diffraction patterns as that of unmodified BSG, indicating no significant change of physical state after modification. The broad peak at 2θ of ˜14° and the absence of any intense peak indicates that all samples were in amorphous state (Rashid, Ahmed, Hussain, Huang, & Ahmad, 2019). Most of biopolymers have very little crystalline region due to low homogeneity. Shi et al. (2017) reported that the esterification of *Acacia seyal* gum with OSA had no significant effect on the gum amorphous state. A broad peak appeared at 2θ of ˜29° in S3 revealed the more amorphous structure. These results are in good agreement with those of Wang and Wang (2002) and Sav, Fule, Ali, and Amin (2013), who mentioned that the esterification reaction occurred primarily in the amorphous regions. Wang et al. (2011) studied the characteristics of OSA-modified starch granules prepared at different degrees of substitution (DS). These researchers reported that the XRD pattern remained unchanged at low degree of substitution (0.19); whereas, increasing DS decreased the ordered structure of starch granules.
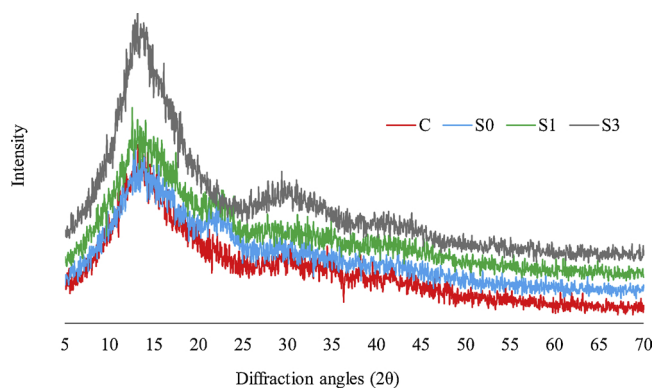
Fig. 4. X-ray diffraction pattern of different BSG samples; C indicates unmodified sample. S0, S1 and S3 indicate the modified samples prepared at OSA:BSG weight ratios of 0, 0.01 and 0.03, respectively.

3.5. Film properties

3.5.1. Physical properties

Different physical properties of modified BSG-based films are reported in Table 2. The film thickness ranged from 55 to 65 μm. A similar value (56 μm) was reported by Khazaei et al. (2014). Modification with OSA had no significant (p > 0.05) influence on the film thickness. BSG modification increased the film density from 1.14 to 1.33 g/cm³. The opacity of biopolymer-based films is related to the microstructure, homogeneity, particle size distribution, the differences in the refractive indices of different ingredients and their variations during drying (Rubilar, Zúñiga, Osorio, & Pedreschi, 2015). Unmodified BSG films had the highest transparency. Modification increased the opacity of BSG films likely through increasing the interactions between biopolymer chains. The moisture content of BSG films was not affected by the modification, indicating that there are still sufficient polar groups along the BSG backbone to make hydrogen bonds with water molecules.

Since the backbone of unmodified BSG was rich in −OH groups, the added water droplet was quickly flattened, giving the lowest contact angle value (Table 2). An increase in the contact angle values was observed after modification, indicating that the OS groups were able to increase the surface hydrophobicity of BSG films. Increasing the extent of modification also reduced the wettability by water molecules. Our results were similar to those reported by Biswas et al. (2009) and Zhou et al. (2009a,b)Zhou, Ren, Tong, Ma et al., 2009Zhou et al. (2009a,b). Water solubility is an important characteristic of edible films and

coatings. High solubility in water is required when the products (e.g., ready to eat edible sachets) are dissolved in water prior to use. However, in most applications, a lower degree of water solubility is of importance in order to protect the packaging integrity against water (Stuchell & Krochta, 1994). The solubility in water of BSG films was reduced significantly (p < 0.05) after modification with OSA which was attributed to the increase in the hydrophobicity. Water vapor transmission is due to the absorption of water molecules to the surface of biopolymer-based films, diffusion through the polymeric network and desorption from the other side. The existence of micro-cracks and pores considerably increases the WVP. Therefore, this parameter can indirectly provide information about the film network (Jiang, Li, Chai, & Leng, 2010; Sebti, Chollet, Degraeve, Noel, & Peyrol, 2007). BSG molecules have large amounts of hydrophilic groups along their backbone, which have the ability to absorb a large number of water molecules. As expected, a decrease in the WVP of BSG films was observed after modification with OSA mainly due to the higher surface hydrophobicity.

Data are the average of at least three independent replicates ± standard deviation. In each row, different lowercase letters indicate significant differences (p < 0.05). C indicates unmodified sample. S0, S1 and S3 indicate the modified samples prepared at OSA:BSG weight ratios of 0, 0.01 and 0.03, respectively.

Physicochemical modifications of film networks through different methods (e.g., incorporating different ingredients) may sometimes change the color as well as the visual appearance (Ghanbarzadeh, Almasi, & Entezami, 2010). As reported in Table 3, the modification with OSA did not result in significant (p < 0.05) changes in Δ*E* (with respect to standard white plate) and *WI* values of different BSG-based films.

Data are the average of at least three independent replicates ± standard deviation. In each column, different lowercase letters indicate significant differences (p < 0.05). C indicates unmodified sample. S0, S1 and S3 indicate the modified samples prepared at OSA:BSG weight ratios of 0, 0.01 and 0.03, respectively.

3.5.2. Mechanical properties

Fig. 5 shows stress-strain curves of different BSG films. The amounts of elongation at break (EAB) and ultimate tensile strength (TS) are summarized in Table 4. A change from brittle to ductile was observed in films with increasing the degree of modification. From a statistical viewpoint, there was a significant increase in TS after modification; while, only a significant difference in the elongation of sample S3 was observed. No significant difference was observed in the elongation of

Table 2
Physical properties of films prepared from different types of BSG.

	C	S0	S1	S3
Thickness (μm)	65 ± 6a	63 ± 4ab	55 ± 4b	57 ± 4ab
WVP (g /h mm kPa) × 10⁶	1.42 ± 0.04a	1.29 ± 0.06b	0.94 ± 0.02c	0.72 ± 0.02d
Opacity (1/mm)	8.46 ± 1.05b	10.51 ± 0.60a	10.32 ± 0.38a	10.76 ± 0.68a
Solubility (%)	56.20 ± 0.77a	50.51 ± 1.38b	41.31 ± 2.20c	24.99 ± 4.02d
Moisture content (%)	12.75 ± 0.98a	13.57 ± 1.18a	13.47 ± 2.42a	12.53 ± 1.41a
Density (g/cm³)	1.14 ± 0.04c	1.21 ± 0.02bc	1.30 ± 0.08ab	1.33 ± 0.05a
Contact angle (º)	46.45 ± 0.90c	46.56 ± 2.33c	54.65 ± 2.23b	71.94 ± 2.67a

Table 3
Color measurements of BSG and modified BSG films.

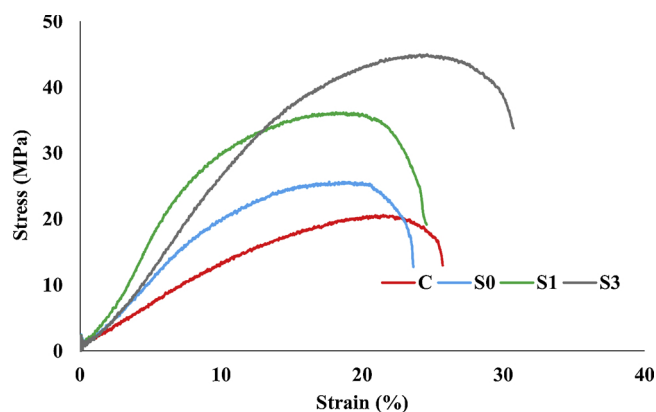| Sample	L^*	a^*	b^*	Δ*E*	*WI*
C	68.33 ± 3.21a	5.00 ± 0.00b	15.33 ± 0.58ab	29.83 ± 2.81a	64.44 ± 2.95a
S0	68.33 ± 3.06a	5.67 ± 0.58ab	16.33 ± 0.58a	30.48 ± 2.38a	63.89 ± 2.56a
S1	68.33 ± 5.03a	5.33 ± 0.58b	14.67 ± 0.58b	29.57 ± 4.62a	64.67 ± 4.80a
S3	72.67 ± 2.52a	6.33 ± 0.58a	14.33 ± 0.58b	25.98 ± 2.21a	68.48 ± 2.33a

Fig. 5. Stress vs. strain curves of different BSG-based films. C indicates unmodified sample; S0, S1 and S3 indicate the modified samples prepared at OSA:BSG weight ratios of 0, 0.01 and 0.03, respectively.

Table 4
Mechanical properties of BSG and modified BSG films.

Sample	Elongation at break (%)	Tensile strength (MPa)
C	25.9 ± 1.8b	21.3 ± 3.0d
S0	23.8 ± 1.6b	26.5 ± 1.5c
S1	24.1 ± 0.1b	37.9 ± 1.2b
S3	36.9 ± 4.1a	46.4 ± 2.8a

samples C, S0 and S1. Taking into account the plasticizing effects of water molecules (as ubiquitous plasticizer molecules in bio-based films) (Hasheminya et al., 2019), the first assumption was that the changes in the mechanical properties were due to the changes in the moisture content. However, the moisture content remained constant after modification (Table 2). Therefore, changes in the mechanical properties could not be attributed to the variations in the amount of water molecules present in the film matrix. The increase in the negative charge along the BSG backbone after modification (data not shown), as a result of the presence of free carboxyl groups (Fig. 1), was likely the main reason for the changes in the mechanical properties via different mechanisms: i) increasing the free spaces between biopolymer chains

resulting from electrostatic and steric repulsions which can increase the film flexibility (Zahedi, Ghanbarzadeh, & Sedaghat, 2010); ii) increasing the linearity of individual biopolymer chains in film network as a result of the electrostatic repulsion between similarly charged adjacent carboxyl groups. The simultaneous increase in the flexibility and ultimate strength of films prepared from S3 is likely a combined effect of the increase in the free spaces between the chains and also the increase in the chain linearity. Formation of new interactions in the network (like hydrophobic interactions between the side chains of OSA) might also have a role. Moreover, two carboxyl functional groups of OSA molecule might also work as a cross-linker between the hydroxyl groups of different biopolymer chains which can reinforce the film network. Ren et al. (2010) reported that the modification of starch-based films could considerably change the mechanical properties. DSA-modified starch-based films were more strong and rigid, while OSA-modified ones were more flexible and ductile. These authors concluded that the reaction of OSA with reactive functional groups along starch molecules was higher than that of DSA (i.e. a higher degree of substitution in the presence of OSA) mainly due to the differences in the alkenyl group chain length. The number of free $-OH$ groups and hence the ability of biopolymer chains to develop hydrogen bonds is reduced at a higher degree of substitution and therefore, an increase in the chain mobility is observed (Ren et al., 2010).

Data are the average of at least three independent replicates ± standard deviation. In each column, different lowercase letters indicate significant differences ($p < 0.05$). C indicates unmodified sample. S0, S1 and S3 indicate the modified samples prepared at OSA:BSG weight ratios of 0, 0.01 and 0.03, respectively.

3.5.3. Film microstructure

SEM micrographs of various BSG-based films are shown in Fig. 6. Generally, a rough surface was observed in the unmodified sample due to the presence of discrete spherical particles. The surface roughness and the number of micro-cracks decreased after modification. A sheet-like and relatively dense structure was observed in the BSG films prepared from sample S3 (Fig. 6d). The cross-sectional view revealed that the sheets were stacked in compact layers (Fig. 6e–f). Changes in the microstructure indicated that the esterification reaction had taken place.
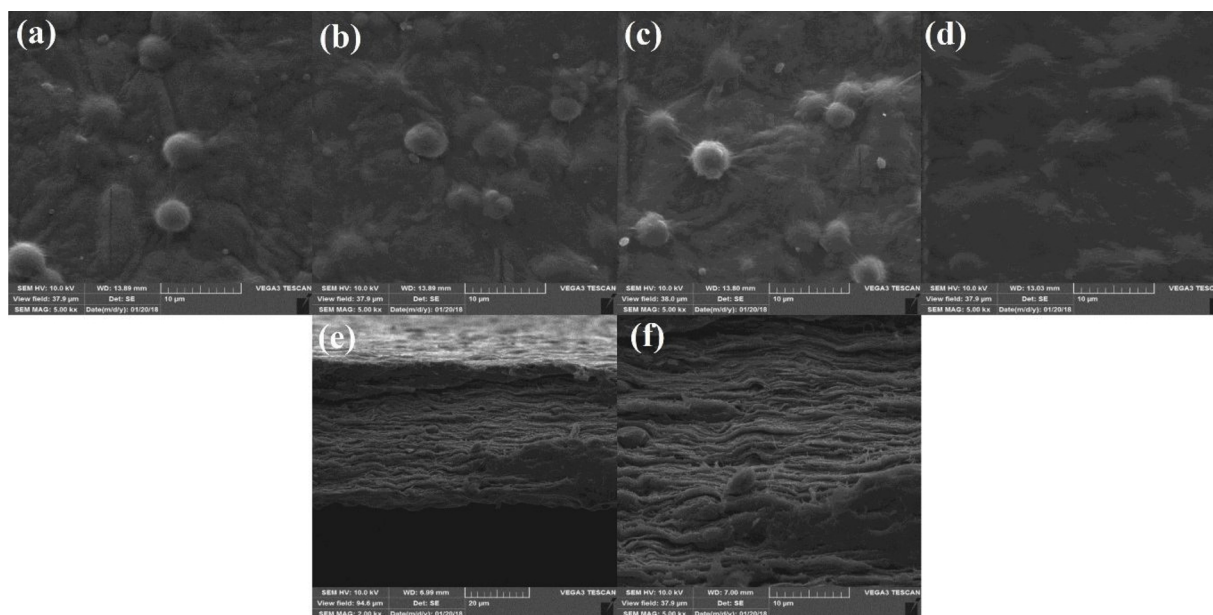

Fig. 6. a–d: Surface SEM micrographs of different BSG-based films prepared from unmodified BSG (C) and those modified at OSA:BSG weight ratios of 0% (S0), 0.01% (S1) and 0.03% (S3), respectively. e–f: the cross-sectional view of films prepared from sample S3 at two magnifications.

4. Conclusion

This study aimed to evaluate the characteristics of BSG films modified with different OSA contents (0, 1%, and 3% based on the weight of basil seed gum). FT-IR revealed that OSA groups were introduced into the BSG molecular structure. Meanwhile, XRD results revealed no significant change of physical state after modification. The contact angle of modified BSG films increased due to the modification with hydrophobic OS groups. The results showed that the physical properties of the films were improved particularly after modification at the WR of 0.03. The microstructural analysis of BSG and modified BSG films revealed the presence of cracks on the surface of C and S0; whereas, a smooth surface was observed for S1 and S3. These results indicate that the OSA-modified BSG has a potential for the production of water-resistant edible films.

Acknowledgment

References

Abiddin, N. Z., Yusoff, A., & Ahmad, N. (2018). Effect of octenylsuccinylation on physicochemical, thermal, morphological and stability of octenyl succinic anhydride (OSA) modified sago starch. *Food Hydrocolloids, 75*, 138–146.

Afshari-Jouybari, H., & Farahnaky, A. (2011). Evaluation of Photoshop software potential for food colorimetry. *Journal of Food Engineering, 106*(2), 170–175.

Ali, U., Bijalwan, V., Basu, S., Kesarwani, A. K., & Mazumder, K. (2017). Effect of β-glucan-fatty acid esters on microstructure and physical properties of wheat straw arabinoxylan films. *Carbohydrate Polymers, 161*, 90–98.

Bai, Y., & Shi, Y.-C. (2011). Structure and preparation of octenyl succinic esters of granular starch, microporous starch and soluble maltodextrin. *Carbohydrate Polymers, 83*(2), 520–527.

Bai, Y., Shi, Y.-C., Herrera, A., & Prakash, O. (2011). Study of octenyl succinic anhydride-modified waxy maize starch by nuclear magnetic resonance spectroscopy. *Carbohydrate Polymers, 83*(2), 407–413.

Benbettaïeb, N., Karbowiak, T., Brachais, C.-H., & Debeaufort, F. (2016). Impact of electron beam irradiation on fish gelatin film properties. *Food Chemistry, 195*, 11–18.

Biswas, A., Selling, G. W., Woods, K. K., & Evans, K. (2009). Surface modification of zein films. *Industrial Crops and Products, 30*(1), 168–171.

Chao, Z., Yue, M., Xiaoyan, Z., & Dan, M. (2010). Development of soybean protein-isolate edible films incorporated with beeswax, span 20, and glycerol. *Journal of Food Science, 75*(6), C493–C497.

Debeaufort, F., Quezada-Gallo, J.-A., & Voilley, A. (1998). Edible films and coatings: Tomorrow's packagings: A review. *Critical Reviews in Food Science, 38*(4), 299–313.

Eenschooten, C., Guillaumie, F., Kontogeorgis, G. M., Stenby, E. H., & Schwach-Abdellaoui, K. (2010). Preparation and structural characterisation of novel and versatile amphiphilic octenyl succinic anhydride–modified hyaluronic acid derivatives. *Carbohydrate Polymers, 79*(3), 597–605.

Esteghlal, S., Niakosari, M., Hosseini, S. M. H., Mesbahi, G. R., & Yousefi, G. H. (2016). Gelatin-hydroxypropyl methylcellulose water-in-water emulsions as a new bio-based packaging material. *International Journal of Biological Macromolecules, 86*, 242–249.

Gahruie, H. H., Ziaee, E., Eskandari, M. H., & Hosseini, S. M. H. (2017). Characterization of basil seed gum-based edible films incorporated with Zataria multiflora essential oil nanoemulsion. *Carbohydrate Polymers, 166*, 93–103.

Ghanbarzadeh, B., Almasi, H., & Entezami, A. A. (2010). Physical properties of edible modified starch/carboxymethyl cellulose films. *Innovative Food Science & Emerging Technologies, 11*(4), 697–702.

Hashemi Gahruie, H. (2019). *Chemical modification of basil seed gum to improve interfacial properties. Ph.D. thesis.* Iran: Department of Food Science and Technology, Shiraz University.

Hasheminya, S.-M., Mokarram, R. R., Ghanbarzadeh, B., Hamishekar, H., Kafil, H. S., & Dehghannya, J. (2019). Development and characterization of biocomposite films made from kefiran, carboxymethyl cellulose and Satureja khuzestanica essential oil. *Food Chemistry, 289*, 443–452.

Hosseini, M., Razavi, S., & Mousavi, M. (2009). Antimicrobial, physical and mechanical properties of chitosan-based films incorporated with thyme, clove and cinnamon essential oils. *Journal of Food Processing and Preservation, 33*(6), 727–743.

Hosseini, S. M. H., Gahruie, H. H., Razmjooie, M., Sepeidnameh, M., Rastehmanfard, M., Tatar, M., et al. (2019). Effects of novel and conventional thermal treatments on the physicochemical properties of iron-loaded double emulsions. *Food Chemistry, 270*, 70–77.

Janjarasskul, T., & Krochta, J. M. (2010). Edible packaging materials. *Annual Review of Food Science and Technology, 1*, 415–448.

Jiang, Y., Li, Y., Chai, Z., & Leng, X. (2010). Study of the physical properties of whey protein isolate and gelatin composite films. *Journal of Agricultural and Food Chemistry, 58*(8), 5100–5108.

Kang, J., Cui, S. W., Chen, J., Phillips, G. O., Wu, Y., & Wang, Q. (2011). New studies on gum ghatti (Anogeissus latifolia) part I. Fractionation, chemical and physical characterization of the gum. *Food Hydrocolloids, 25*(8), 1984–1990.

Khazaei, N., Esmaiili, M., Djomeh, Z. E., Ghasemlou, M., & Jouki, M. (2014). Characterization of new biodegradable edible film made from basil seed (Ocimum basilicum L.) gum. *Carbohydrate Polymers, 102*, 199–206.

Konwar, A., Gogoi, N., Majumdar, G., & Chowdhury, D. (2015). Green chitosan–carbon dots nanocomposite hydrogel film with superior properties. *Carbohydrate Polymers, 115*, 238–245.

Meng, F., Zheng, L., Wang, Y., Liang, Y., & Zhong, G. (2014). Preparation and properties of konjac glucomannan octenyl succinate modified by microwave method. *Food Hydrocolloids, 38*, 205–210.

Mohammadi, S., Abbasi, S., & Scanlon, M. (2016). Development of emulsifying property in Persian gum using octenyl succinic anhydride (OSA). *International Journal of Biological Macromolecules, 89*, 396–405.

Nie, S.-P., Wang, C., Cui, S. W., Wang, Q., Xie, M.-Y., & Phillips, G. O. (2013). The core carbohydrate structure of Acacia seyal var. seyal (Gum arabic). *Food Hydrocolloids, 32*(2), 221–227.

Pan, J., Yang, L., & Qiu, D. (2015). Optimization of a synthesis process for octenylsuccinic anhydride modified gum arabic. *Food Science and Biotechnology, 24*(1), 7–13.

Rashid, F., Ahmed, Z., Hussain, S., Huang, J.-Y., & Ahmad, A. (2019). Linum usitatissimum L. seeds: Flax gum extraction, physicochemical and functional characterization. *Carbohydrate Polymers, 215*, 29–38.

Ren, L., Jiang, M., Tong, J., Bai, X., Dong, X., & Zhou, J. (2010). Influence of surface esterification with alkenyl succinic anhydrides on mechanical properties of corn starch films. *Carbohydrate Polymers, 82*(3), 1010–1013.

Ren, L., Wang, Q., Yan, X., Tong, J., Zhou, J., & Su, X. (2016). Dual modification of starch nanocrystals via crosslinking and esterification for enhancing their hydrophobicity. *Food Research International, 87*, 180–188.

Rubilar, J. F., Zúñiga, R. N., Osorio, F., & Pedreschi, F. (2015). Physical properties of emulsion-based hydroxypropyl methylcellulose/whey protein isolate (HPMC/WPI) edible films. *Carbohydrate Polymers, 123*, 27–38.

Sagiri, S., Behera, B., Rafanan, R., Bhattacharya, C., Pal, K., Banerjee, I., et al. (2014). Organogels as matrices for controlled drug delivery: A review on the current state. *Soft Materials, 12*(1), 47–72.

Sav, A. K., Fule, R. A., Ali, M. T., & Amin, P. (2013). Synthesis and evaluation of octenyl succinate derivative of fenugreek gum as extended release polymer. *Journal of Pharmaceutical Investigation, 43*(5), 417–429.

Sebti, I., Chollet, E., Degraeve, P., Noel, C., & Peyrol, E. (2007). Water sensitivity, antimicrobial, and physicochemical analyses of edible films based on HPMC and/or chitosan. *Journal of Agricultural and Food Chemistry, 55*(3), 693–699.

Shi, Y., Li, C., Zhang, L., Huang, T., Ma, D., Tu, Z.-c., et al. (2017). Characterization and emulsifying properties of octenyl succinate anhydride modified Acacia seyal gum (gum arabic). *Food Hydrocolloids, 65*, 10–16.

Stuchell, Y. M., & Krochta, J. M. (1994). Enzymatic treatments and thermal effects on edible soy films. *Journal of Food Science, 59*(6), 1332–1337.

Testing, A. S. f., & Materials (2013). *Standard test methods for water vapor transmission of materials.* ASTM International.

Thakur, R., Saberi, B., Pristijono, P., Golding, J., Stathopoulos, C., Scarlett, C., et al. (2016). Characterization of rice starch-ι-carrageenan biodegradable edible film. Effect of stearic acid on the film properties. *International Journal of Biological Macromolecules, 93*, 952–960.

Wang, Y. J., & Wang, L. (2002). Characterization of acetylated waxy maize starches prepared under catalysis by different alkali and alkaline-earth hydroxides. *Starch-Stärke, 54*(1), 25–30.

Wang, X., Li, X., Chen, L., Xie, F., Yu, L., & Li, B. (2011). Preparation and characterisation of octenyl succinate starch as a delivery carrier for bioactive food components. *Food Chemistry, 126*(3), 1218–1225.

Xu, H., Canisag, H., Mu, B., & Yang, Y. (2015). Robust and flexible films from 100% starch cross-linked by biobased disaccharide derivative. *ACS Sustainable Chemistry & Engineering, 3*(11), 2631–2639.

Yang, W., Bian, H., Jiao, L., Wu, W., Deng, Y., & Dai, H. (2017). High wet-strength, thermally stable and transparent TEMPO-oxidized cellulose nanofibril film via crosslinking with poly-amide epichlorohydrin resin. *RSC Advances, 7*(50), 31567–31573.

Zahedi, Y., Ghanbarzadeh, B., & Sedaghat, N. (2010). Physical properties of edible emulsified films based on pistachio globulin protein and fatty acids. *Journal of Food Engineering, 100*(1), 102–108.

Zhou, J., Ren, L., Tong, J., & Ma, Y. (2009). Effect of surface esterification with octenyl succinic anhydride on hydrophilicity of corn starch films. *Journal of Applied Polymer Science, 114*(2), 940–947.

Zhou, J., Ren, L., Tong, J., Xie, L., & Liu, Z. (2009). Surface esterification of corn starch films: Reaction with dodecenyl succinic anhydride. *Carbohydrate Polymers, 78*(4), 888–893.

Zúñiga, R., Skurtys, O., Osorio, F., Aguilera, J., & Pedreschi, F. (2012). Physical properties of emulsion-based hydroxypropyl methylcellulose films: Effect of their microstructure. *Carbohydrate Polymers, 90*(2), 1147–1158.